Under-gapped SWIFT

Michael Tesch[1], Steen Moeller[1], Ryan Chamberlain[1], and Michael Garwood[1]
[1]*CMRR, University of Minnesota, Minneapolis, MN, United States*

TARGET AUDIENCE

With its short acquisition delay between radiofrequency (RF) pulse elements and data acquisition periods, SWIFT is well-suited for imaging short-T2 species such as cortical bone. Its main limiting factor is the “dead-time” required to switch between transmit and receive modes; while typically less than 3 us on research systems, this switching time is much longer on clinical systems where it presents a significant challenge to SWIFT’s implementation. Here, and under-gapped version of SWIFT is investigated for its potential to accommodate the dead-times typical of clinical scanners.

PURPOSE

The aim of this work is to address limitations of SWIFT arising from the hard-minimum dead-time required by scanner hardware. This minimum limits readout bandwidth and consumes valuable time that could be used for RF excitation and/or signal acquisition. In SWIFT, the excitation pulse is interleaved with the acquisition readout. In practice, this is accomplished by toggling the T/R switch back and forth between transmit and receive modes during a frequency-swept pulse. Conventionally, a flat excitation profile is maintained by inserting gaps at a frequency equal to the sweep width of the pulse, which is also the FOV bandwidth. This particular gap spacing creates excitation sidebands (aliases) whose edges just meet the edge of the baseband excited by the frequency sweep, but lie beyond the FOV. Each of these gaps requires dead-time at both beginning and end to allow the RF chain to switch back and forth between transmit and receive modes. At high bandwidths, this dead-time limits how much time can be spent transmitting and receiving. This work demonstrates a method for collapsing gaps, making more time available for some combination of: T/R switching, longer pulse elements thus reducing SAR, longer sampling to improve SNR, or scaling-down the length of pulse and acquisition to increase the max possible bandwidth.

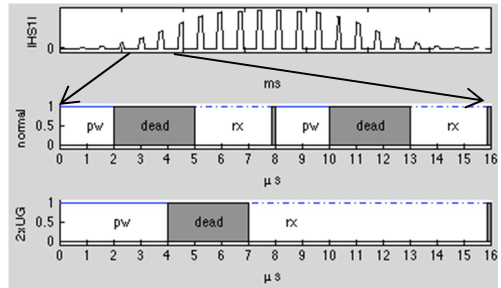

Fig 1. Gapped RF pulse in SWIFT, the first row shows the full pulse with acquisition gaps, for 125 kHz FOV, the second row shows detailed gap timing for two gap periods in normal SWIFT, and the bottom row shows timing for the same period under-gapped. *pw* denotes RF transmit pulse element, *dead* denotes T/R switching time, and *rx* denotes receiver gate open. Undergapping eliminates the dead time from every second pulse element. Here dw=8 us, and the dead time is 3 us. In undergapped SWIFT (lower row) the pulse element length is doubled while the second pw and dead time from the second dw has been converted to receiver-open time denoted ‘rx’. This conversion is repeated for every two dwell-times throughout the pulse; in this case adding 20% more useful time.

METHODS

By inserting gaps less frequently than the pulse bandwidth, the excitation profile becomes distorted by impinging sidebands. Choosing a gap frequency half of the excitation frequency limits this distortion to two components: a sinusoidal modulation and a discontinuity at the center of the excitation where the sidebands meet. The sinusoidal modulation is mitigated by alternation between even and odd gap collapse, such that the excitation profile of an even-gapped plus an odd-gapped pulse is nearly flat (Fig. 2). SWIFT recon has been done by deconvolution[1] or inverse solution of a signal model[3]. A signal model matrix E is calculated using Bloch simulation for the pair of pulses, the rows being discretized in time and the columns discretizing space, simiar to[3]. Thus the experiment is described by s=Eρ, where s is the readout and ρ is the spin density. A regularized solution to min ρ {||Eρ – s|| + L||ρ||} produces an object profile to be fourier transformed into an FID for radial gridding reconstruction. This approach accomodates band restriction and explicit choice of which readout data-points are incorporated.

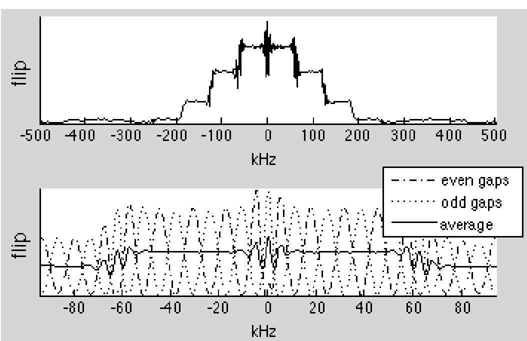

Figure 2. Simulation showing flip angle across a 125 kHz FOV resulting from under-gapping. Top row shows the broad side-bands created by gapping, bottom row shows detail of the baseband from even or odd gaps and the averaging of these, achieved by alternation.

RESULTS

Figure 3 is an image of a breast phantom at 125 kHz FOV and 62.5 kHz gap rate. The object is well delineated, but there are still some radial artifacts visible.

DISCUSSION

This method removes half of the dead-time requirements of SWIFT, greatly increasing the maximum bandwidth. Primarily it is a way to mix swept-frequency pulses with non-flat excitation profiles to generate the flat excitation profile necessary for imaging and combine the readouts from these to reconstruct a profile. Work is needed to address a glitch at the center of the FOV arising from interference between the overlapping excitation bands. This might be done through various pulse optimization techniques to reshape the excitation profile. There are also some low-frequency ring-like artifacts whose effect on relaxation is not yet clear.

CONCLUSION

Eliminating half of the dead-time in SWIFT allows some combination of the following advantages, depending on experimental requirements, relative to normal gapped SWIFT: higher bandwidths, higher flip angles, better SNR, lower SAR. An ultimate goal is to implement SWIFT on a clinical scanner, where limitations on T/R and coil switching times are significantly longer than on the pre-clinical systems used to develop SWIFT.

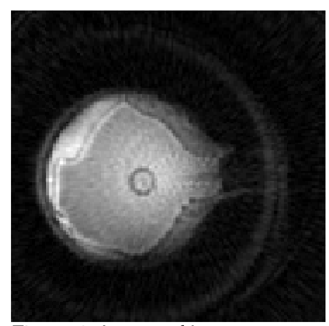

Figure 3. Image of breast phantom, acquisition parameters were: 16k radial views, resolution=192^3, fa=5, TR=8 µs, 125 kHz bandwidth, 62.5 kHz gapping.

REFERENCES

1. Idiyatullin D, Corum C, Park JY, Garwood M. Fast and quiet MRI using a swept radiofrequency. *J Magn Res*, 181(2):342–349.
2. Kuethe DO, Caprihan A, Lowe IJ, Madio DP, Gach HM. Transforming NMR Data Despite Missing Points. *J Magn Res*, 139(1):18–25.
3. Weiger M, Hennel F, Pruessmann KP. Sweep MRI with algebraic reconstruction. *Magn Res Med*, 64(6):1685–1695.

The following NIH grants supported this work: P41 EB015894, P41 RR008079, S10 RR023730, S10 RR027290.